

Blue light-emitting polyfluorenes containing dibenzothiophene-*S,S*-dioxide unit in alkyl side chain

Yiwen Fang, Jie Liu, Yuhao Zhang, Ting Guo*, Fei Huang, Wei Yang* & Yong Cao

Institute of Polymer Optoelectronic Materials and Devices, State Key Laboratory of Luminescent Materials and Devices, South China University of Technology, Guangzhou 510640, China

Received March 24, 2017; accepted June 15, 2017; published online September 13, 2017

Blue light-emitting polyfluorenes containing dibenzothiophene-*S,S*-dioxide (SO) unit in alkyl side chain (**PF-FSOs** and **PF-CzSOs**) were synthesized. All the polymers show high thermal stability with the decomposition temperatures over 400 °C. The highest occupied molecular orbital (HOMO) and the lowest unoccupied molecular orbital (LUMO) energy levels of the copolymer slightly decrease with the increase of SO content in side chain. PL spectra of the polymers show slightly red shift and broadening with the increase of solvent polarities, indicating unremarkable intramolecular charge transfer (ICT) effect in the polymers containing SO unit in alkyl side chain. EL spectra of the polymers are almost unchanged in the current densities from 100 to 400 mA cm⁻², indicating the superb EL stability of the resulted polymers. The EL spectra of the copolymers exhibit obvious blue-shift and narrowing with the CIE of (0.18, 0.11) for **PF-FSO10** and (0.17, 0.11) for **PF-CzSO10**, respectively, compared with **PF-SO10** containing SO unit in main chain with the CIE of (0.16, 0.17) and **PFO** with the CIE of (0.18, 0.18). The superior device performances were obtained with the luminous efficiency (LE_{max}) of 1.17 and 0.68 cd A⁻¹ for **PF-FSO15** and **PF-CzSO20**, respectively, compared with the LE_{max} of 0.37 cd A⁻¹ for **PFO**. The results indicate that linking SO unit to alkyl side chain of the polyfluorene is a promising strategy for efficient blue light-emitting polymers.

dibenzothiophene-*S,S*-dioxide, alkyl side chain, polyfluorene, blue emission, polymer light-emitting diode (PLED)

Citation: Fang Y, Liu J, Zhang Y, Guo T, Huang F, Yang W, Cao Y. Blue light-emitting polyfluorenes containing dibenzothiophene-*S,S*-dioxide unit in alkyl side chain. *Sci China Chem*, 2017, 60, doi: 10.1007/s11426-017-9100-0

1 Introduction

Recently, polymer light-emitting diodes (PLEDs) have attracted considerable attention due to their great potential application in full-color flat-panel displays and solid-state lightings based on large area flexible substrates [1–4]. Among the currently available conjugated polymers as the emissive layer for PLEDs, the application of red and green light-emitting polymers has reached the industrial production standard [5–7]. Then blue light-emitting polymers remain a great challenge for full-color display in terms of lower quantum ef-

iciency and color stability [8–10]. As one of the most extensively investigated blue light-emitting polymers, polyfluorene (PF) has been regarded as a potential blue-emitting polymers owing to the high photoluminescent quantum yield (PLQY), good charge transport property, outstanding thermal stability, and versatile molecular structures modifying strategies [11–13]. However, the light emitting diodes fabricated from polyfluorene always suffer from a degradation of the device under thermal annealing or upon long-term operation, which induces color impurity [14,15]. And the efficiency is limited by the intrinsic disadvantage of unbalanced transport of electrons and holes. Many efforts have been made to address such drawbacks [16,17]. One effective way is to incorporate various electron-deficient moieties into the polymer

*Corresponding authors (email: mstguo@scut.edu.cn; pswyang@scut.edu.cn)

backbone, which can improve the efficiency and color purity of blue light-emitting polymers [18–20].

The dibenzothiophene-*S,S*-dioxide (SO) unit is topologically similar to fluorene and carbazole moiety by replacing carbon or nitrogen atom with a $-\text{SO}_2-$ group, turning it into an electron-deficient moiety with high electron affinity and high fluorescent efficiency [21–23]. Recently, SO derivatives were incorporated into small molecules and polymers to improve the electron injection/transportation ability and simultaneously achieve high-efficiency blue light emitter [24–26]. Specially, the fluorene-based polymers embodying SO unit have obtained high device efficiencies [27–32]. For example, the spectral stability and luminous efficiency of the blue-emitting polyfluorenes were significantly improved via incorporating of SO isomer (3,7-diyl or 2,8-diyl) into the polyfluorene backbone [24]. The solubility and the color purity were improved via introducing 2,8-dioctyldibenzothiophene-*S,S*-dioxide (DOSO) unit in the polyfluorene backbone [25]. While the intramolecular charge transfer (ICT) effect existed in the polymers containing SO unit in the main chain cause the red shift and broadening PL spectra, and further result in the color impurity in blue emission [26].

Up to date, the reported light-emitting polymers containing SO unit were almost based on the SO unit in main chain, although the β -phase was induced by grafting the SO unit of 1 mol% in the side chain of poly(9,9-dioctylfluorene) [30]. The polymers linked SO unit in alkyl side chain keep a certain distance between the backbone donor and SO acceptor, which probably could restrain the ICT effect. Herein, the polyfluorenes containing SO unit linked to the alkyl side chain of fluorene and carbazole moieties were synthesized and investigated, respectively.

2 Experimental

2.1 Materials

Solvents (THF and toluene) were purified and freshly distilled prior to use according to the reported procedure. All reagents, unless otherwise specified, were obtained from Aldrich (USA), Acros (Belgium), or TCI Chemical Co. (Japan) and used as received. All manipulations involving air-sensitive reagents were performed under an atmosphere of dried argon. 2-Bromo-dibenzo [*b,d*] thiophene (**1**), 2-(8-bromohexyl) dibenzo [*b,d*] thiophene (**2**), 2-(8-bromohexyl) dibenzo [*b,d*] thiophene-5,5-dioxide (**3**), 2,7-dibromo-9-octyl-9*H*-fluorene (**4**) and 3,6-dibromocarbazole (**6**), 2,7-bis(4,4,5,5-tetramethyl-1,3,2-dioxaborolan-2-yl)-9,9-dioctylfluorene (**8**), 2,7-dibromo-9,9-dioctylfluorene (**9**) and 3,7-dibromo-dibenzothiophene-*S,S*-dioxide (**10**) were synthesized according to the reported procedures [33–35].

2.1.1 Synthesis of monomers

(1) 2-(6-(2,7-Dibromo-9-octyl-9*H*-fluoren-9-yl)hexyl)di-

benzo [*b,d*] thiophene 5,5-dioxide (**5**)

2,7-Dibromo-9-octyl-9*H*-fluorene (5 g, 11.46 mmol), tetra-*n*-butylammonium bromide (184.75 mg, 573.10 mmol) and dimethyl sulphoxide (DMSO) (50 mL) were added into reaction vessel, then NaOH (2.29 g, 57.31 mmol) aqueous solution was added into mixture and stirring at room temperature for 2 h, 2-(8-bromohexyl) dibenzo [*b,d*] thiophene 5,5-dioxide (4.35 g, 11.46 mmol) was added into mixture and stirring for 24 h at room temperature. The reaction was extracted 3 times by using dichloromethane. After removing the organic phase under reduced pressure, the crude product was purified by column chromatography with a yield of 87%. ^1H NMR (500 MHz, CDCl_3) δ (ppm): 7.81 (dd, 2H), 7.71 (d, 1H), 7.66 (t, 1H), 7.61–7.45 (m, 8H), 7.24 (d, 1H), 2.63 (t, 2H), 1.92 (m, 4H), 1.49 (m, 2H), 1.29–1.20 (br, 14H), 0.83 (m, 3H), 0.60 (br, 4H). ^{13}C NMR (125 MHz, CDCl_3) δ (ppm): 150.02, 144.18, 140.06, 137.65, 134.86, 134.26, 133.53, 130.91, 130.78, 130.63, 129.64, 128.67, 128.0, 122.53, 122.45, 121.70, 43.82, 36.05, 31.26, 30.21, 29.25, 24.46.

(2) 2-(6-(3,6-Dibromo-9*H*-carbazole-9-yl)hexyl) dibenzo [*b,d*] thiophene 5,5-dioxide (**7**)

3,6-Dibromocarbazole (3.72 g, 11.46 mmol), tetra-*n*-butylammonium bromide (184.75 mg, 573.10 mmol) and DMSO (50 mL) were added into reaction vessel, then NaOH (2.29 g, 57.31 mmol) aqueous solution was added into mixture and stirring at room temperature for 2 h, 2-(8-bromohexyl) dibenzo [*b,d*] thiophene 5,5-dioxide (4.35 g, 11.46 mmol) was added into mixture and stirring for 24 h at room temperature. The reaction was extracted 3 times by using dichloromethane. After removing the organic phase under reduced pressure, the crude product was purified by column chromatography with a yield of 90%. ^1H NMR (500 MHz, CDCl_3) δ (ppm): 8.45 (d, 2H), 7.82 (d, 1H), 7.66–7.60 (dd, 2H), 7.63 (m, 1H), 7.56–7.52 (m, 4H), 7.27 (d, 3H), 4.27–4.22 (t, 2H), 2.68–2.63 (t, 2H), 1.87–1.82 (br, 2H), 1.63–1.58 (br, 2H), 1.36–1.26 (m, 4H). ^{13}C NMR (125 MHz, CDCl_3) δ (ppm): 149.30, 139.18, 138.11, 135.19, 133.69, 131.80, 131.59, 130.33, 130.19, 128.96, 123.35, 123.18, 122.02, 121.99, 121.97, 121.38, 121.30, 111.92, 110.31, 43.14, 35.91, 30.79, 28.74, 28.67, 26.96.

2.1.2 Synthesis of the polymers

General procedures of Suzuki copolymerization, taking **PF-FSO5** as an example.

Under an argon atmosphere, monomer **8** (321.3 mg, 0.5 mmol), **9** (246.8 mg, 0.45 mmol), **5** (36.6 mg, 0.05 mmol), palladium acetate ($\text{Pd}(\text{OAc})_2$) (3.4 mg, 0.015 mmol) and tricyclohexylphosphine (PCy_3) (8.4 mg, 0.03 mmol) were added to toluene solvent. The solution was stirred and heated up to 80 °C. After the solution became clear, tetraethyl ammonium hydroxide (Et_4NOH) (20% aq, 4 mL) was added. The temperature was kept in the range of 80–85 °C, and the solution was allowed to stir

vigorously for 36 h. The reaction was end-capped by adding phenylboronic acid (0.05 g, 0.4 mmol) and allowed to stir for 12 h. Then bromobenzene (0.125 g, 0.8 mmol) was added followed by stirring for another 12 h. After cooling, the mixtures were precipitated into methanol (150 mL) and filtered. The collected solids were re-dissolved in dichloromethane and washed 3 times with de-ionized water. The organic phase was concentrated under reduced pressure, followed by re-precipitation in methanol. The crude product was further purified by Soxhlet extraction by methanol and acetone successively. The target polymer was collected after drying under vacuum with a yield of 65%. ^1H NMR (500 MHz, CDCl_3) δ (ppm): 7.88 (br, ArH), 7.74 (br, ArH), 2.15 (br, CH_2), 1.28–1.05 (br, CH_2), 0.84 (t, CH_3). Elemental analysis calcd (%) for $[(\text{C}_{29}\text{H}_{40})_{0.95}(\text{C}_{39}\text{H}_{42}\text{O}_2\text{S})_{0.05}]$: C 89.10, H 10.09, S 0.40; found: C 88.62, H 10.73, S 0.71.

PFO: monomer **8** (321.3 mg, 0.5 mmol) and **9** (274.2 mg, 0.5 mmol), yield: 76%. ^1H NMR (500 MHz, CDCl_3) δ (ppm): 7.85–7.84 (br, ArH), 7.71–7.68 (br, ArH), 2.21 (br, CH_2), 1.22–1.44 (br, CH_2), 0.83–0.80 (br, CH_3). Elemental analysis calcd (%) for $[(\text{C}_{29}\text{H}_{40})]$: C 89.69, H 10.31; found: C 88.34, H 10.13.

PF-SO10: monomer **8** (321.3 mg, 0.5 mmol), **9** (219 mg, 0.40 mmol) and **10** (37.4 mg, 0.10 mmol), yield: 68%. ^1H NMR (500 MHz, CDCl_3) δ (ppm): 8.12 (s, Ar-H), 7.88 (br, 2H), 7.68 (br, 4H), 2.14 (br, 4H), 1.16–1.01 (m, 24H), 0.78 (br, 6H); elemental analysis calcd (%) for $[(\text{C}_{29}\text{H}_{40})_{0.90}(\text{C}_{12}\text{H}_6\text{O}_2\text{S})_{0.10}]$: C 88.40, H 9.88, S 0.86; found: C 87.66, H 9.51, S 0.73.

PF-FSO10: monomer **8** (321.3 mg, 0.5 mmol), **9** (219.4 mg, 0.4 mmol) and **5** (73.3 mg, 0.10 mmol), yield: 69%. ^1H NMR (500 MHz, CDCl_3) δ (ppm): 7.89 (br, ArH), 7.74–7.50 (br, ArH), 2.15 (br, CH_2), 1.57–1.05 (br, CH_2), 0.84 (t, CH_3). Elemental analysis calcd (%) for $[(\text{C}_{29}\text{H}_{40})_{0.90}(\text{C}_{39}\text{H}_{42}\text{O}_2\text{S})_{0.10}]$: C 88.54, H 9.89, S 0.79; found: C 88.13, H 10.43, S 1.02.

PF-FSO15: monomer **8** (321.3 mg, 0.5 mmol), **9** (192.0 mg, 0.35 mmol) and **5** (109.9 mg, 0.15 mmol), yield: 62%. ^1H NMR (500 MHz, CDCl_3) δ (ppm): 7.88 (br, ArH), 7.74–7.49 (br, ArH), 2.61 (br, CH_2), 2.16 (br, CH_2), 1.57–1.17 (br, CH_2), 0.84 (t, CH_3). Elemental analysis calcd (%) for $[(\text{C}_{29}\text{H}_{40})_{0.85}(\text{C}_{39}\text{H}_{42}\text{O}_2\text{S})_{0.15}]$: C 88.00, H 9.69, S 1.15; found: C 87.30, H 11.09, S 1.27.

PF-FSO20: monomer **8** (321.3 mg, 0.5 mmol), **9** (164.5 mg, 0.3 mmol) and **5** (146.5 mg, 0.2 mmol), yield: 73%. ^1H NMR (500 MHz, CDCl_3) δ (ppm): 7.88 (br, ArH), 7.72–7.50 (br, ArH), 2.61 (br, CH_2), 2.16 (br, CH_2), 1.57 (br, CH_2), 1.18 (br, CH_2), 0.84 (t, CH_3). Elemental analysis calcd (%) for $[(\text{C}_{29}\text{H}_{40})_{0.80}(\text{C}_{39}\text{H}_{42}\text{O}_2\text{S})_{0.20}]$: C 87.49, H 9.50, S 1.51; found: C 86.85, H 11.01, S 1.94.

PF-CzSO5: monomer **8** (321.3 mg, 0.5 mmol), **9** (246.8 mg, 0.45 mmol) and **7** (31.2 mg, 0.05 mmol), yield: 63%. ^1H NMR (500 MHz, CDCl_3) δ (ppm): 7.88 (br,

ArH), 7.79–7.57 (brm, ArH), 2.16 (br, CH_2), 1.28–1.04 (br, CH_2), 0.84 (br, CH_3). Elemental analysis calcd (%) for $[(\text{C}_{29}\text{H}_{40})_{0.95}(\text{C}_{30}\text{H}_{25}\text{O}_2\text{NS})_{0.05}]$: C 88.99, H 10.02, S 0.41; found: C 88.31, H 11.62, S 0.57.

PF-CzSO10: monomer **8** (321.3 mg, 0.5 mmol), **9** (219.4 mg, 0.40 mmol) and **7** (62.3 mg, 0.10 mmol), yield: 68%. ^1H NMR (500 MHz, CDCl_3) δ (ppm): 8.54 (s, ArH), 7.89 (brm, ArH), 7.79–7.55 (brm, ArH), 2.16 (br, CH_2), 1.28–1.05 (br, CH_2), 0.84 (br, CH_3). Elemental analysis calcd (%) for $[(\text{C}_{29}\text{H}_{40})_{0.90}(\text{C}_{30}\text{H}_{25}\text{O}_2\text{NS})_{0.10}]$: C 88.29, H 9.73, S 0.81; found: C 87.26, H 10.14, S 1.15.

PF-CzSO15: monomer **8** (321.3 mg, 0.5 mmol), **9** (192.0 mg, 0.35 mmol) and **7** (93.5 mg, 0.15 mmol), yield: 75%. ^1H NMR (500 MHz, CDCl_3) δ (ppm): 8.54 (s, ArH), 7.89 (brm, ArH), 7.79–7.71 (brm, ArH), 7.64–7.53 (brm, ArH), 2.16 (br, CH_2), 1.28–1.05 (br, CH_2), 0.84 (br, CH_3). Elemental analysis calcd (%) for $[(\text{C}_{29}\text{H}_{40})_{0.85}(\text{C}_{30}\text{H}_{25}\text{O}_2\text{NS})_{0.15}]$: C 87.61, H 9.45, S 1.20; found: C 87.33, H 10.08, S 1.29.

PF-CzSO20: monomer **8** (321.3 mg, 0.5 mmol), **9** (164.5 mg, 0.3 mmol) and **7** (124.6 mg, 0.2 mmol), yield: 70%. ^1H NMR (500 MHz, CDCl_3) δ (ppm): 8.54 (s, ArH), 7.86–7.71 (brm, ArH), 7.64–7.57 (brm, ArH), 2.74 (br, CH_2), 2.16 (br, CH_2), 1.71 (br, CH_2), 1.50 (br, CH_2), 1.17 (br, CH_2), 0.84 (br, CH_3). Elemental analysis calcd (%) for $[(\text{C}_{29}\text{H}_{40})_{0.80}(\text{C}_{30}\text{H}_{25}\text{O}_2\text{NS})_{0.20}]$: C 83.97, H 9.18, S 1.59; found: C 86.51, H 9.53, S 1.97.

2.2 Measurements

Nuclear magnetic resonance (NMR) spectra were recorded on a Bruker DRX 500 spectrometer (operating at 500 MHz for ^1H NMR, and 125 MHz for ^{13}C NMR, Germany) in deuterated chloroform solution, tetramethylsilane was used as the reference. Elemental analysis was performed on a Vario EL Elemental Analysis Instrument (Elementar Co., Germany). Number-average (M_n) molecular weights were determined by using a Waters GPC 2410 instrument (USA) in tetrahydrofuran (THF) via a calibration curve of polystyrene standards. Differential scanning calorimetry (DSC) measurements were carried out on a Netzsch DSC 204 (Germany) at a heating rate of $10\text{ }^\circ\text{C min}^{-1}$ under N_2 . Thermal gravimetric analysis (TGA) was carried out in a Netzsch TGA-209 thermal analyzer. All measurements were carried out under N_2 with a heating rate of $20\text{ }^\circ\text{C min}^{-1}$. Cyclic voltammetry (CV) was measured by using a CHI660A electrochemical work-station. The measurement was performed at a scan rate of 50 mV s^{-1} at room temperature under the inert atmosphere of Ar. The tetra-(*n*-butyl) ammonium hexafluorophosphate (*n*-Bu₄NPF₆, 0.1 M) in acetonitrile solution was selected as the electrolyte. UV-Vis absorption spectra of polymers in both dilute toluene solution and as thin films were recorded with a HP 8453 spectrophotometer (USA). Photoluminescence (PL) spectra were recorded with a Spex Fluorolog-3

spectrofluorometer (Japan). Photoluminescence (PL) efficiencies were determined in an IS080 integrating sphere (Labsphere, USA) with 325 nm excitation of a HeCd laser (Mells Griot, USA). PL and EL spectra were recorded on an Instaspec IV CCD spectrophotometer (Oriel Co., UK). The morphology of polymer was characterized by a tapping mode atomic force microscopy (AFM), which consists a Seiko SPA 400 (Japan) equipped with an SPI 3800 probe station. The films were spin-coated from xylene solution on the top of the prefabricated poly(styrenesulfonic acid) (PEDOT:PSS) layer.

2.3 Device fabrication and characterization

The obtained polymers were dissolved in *p*-xylene and filtered with a 0.45 mm PTFE filter. Patterned ITO coated glass substrates were cleaned with acetone, detergent, distilled water and 2-propanol followed by ultra-sonication. After treatment with oxygen plasma, 50 nm of poly(3,4-ethylenedioxythiophene) doped with PEDOT:PSS (Batron-P 4083, Bayer AG, Germany) was spin-coated onto the cleaned ITO substrates followed by drying on a hot plate at 120 °C for 20 min. The films of copolymers were coated on the top of the prefabricated PEDOT:PSS layer by spin-casting in a nitrogen-filled glove box. The film thickness of the active layers was around 75–80 nm, as estimated by an Alfa Step 500 surface profiler (Tencor, USA). Finally, 1.5 nm of CsF followed by 120 nm of aluminum (thickness monitored with a STM-100/MF-Sycon quartz crystal) were subsequently evaporated on the top of the light-emitting copolymer layer in a vacuum of 3×10^{-4} Pa.

The hole-/electron-only devices were used as ITO/PEDOT:PSS (40 nm)/polymer (80 nm)/MoO₃ (10 nm)/Al and ITO/ZnO (40 nm)/polymer (80 nm)/CsF (1.5 nm)/Al, respectively. To fabricate the hole-only device, a layer of MoO₃ (10 nm) instead of cesium fluoride was thermally deposited

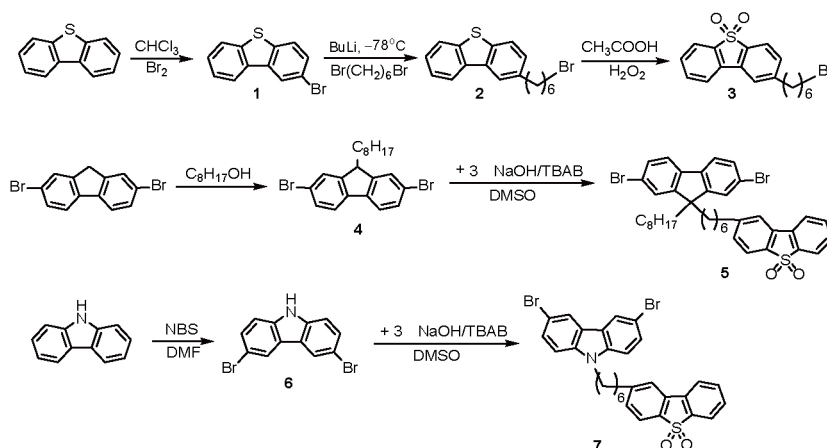
on top of the emission layer with a protective aluminum layer, with the remaining steps the same as those for the bipolar device. For the electron-only device, ITO glass was deposited with a layer of zinc oxide (40 nm) to replace the PEDOT:PSS film, then a thick copolymer layer (80 nm) was spin-cast from *p*-xylene solution on top of the zinc oxide layer and annealed at 100 °C for 20 min. Profilometry (Tencor Alfa-Step 500) was used to determine the thickness of the films. Finally, 1.5 nm of CsF followed by 100 nm of aluminum (thickness monitored with a STM-100/MF Sycon quartz crystal) were thermally evaporated through a shadow mask at a base pressure of 3.0×10^{-4} Pa to form the cathode.

3 Results and discussion

3.1 Synthesis and characterization

The detailed synthetic routes of monomers are shown in Scheme 1. Compound 2-bromo-dibenzo [*b,d*] thiophene (**1**) was synthesized by bromination using liquid bromine as bromine source. 2-(8-Bromohexyl) dibenzo [*b,d*] thiophene (**2**) was synthesized based on the alkylation reaction of monomer **1** and 1,6-dibromohexyl at ultralow temperature. Compound 2-(8-bromohexyl) dibenzo [*b,d*] thiophene-5,5-dioxide (**3**) was prepared in a high yield of 89% based on an oxidizing reaction using hydrogen peroxide as the oxidizer. 2-(6-(2,7-Dibromo-9-octyl-9*H*-fluoren-9-yl)hexyl) dibenzo [*b,d*] thiophene 5,5-dioxide (**5**) was prepared based on the reaction of monomer **3** and **4** under air atmosphere in DMSO solution with a yield of 87%. The same synthetic method was used for the preparation of 2-(6-(3,6-dibromo-9*H*-carbazole-9-yl) hexyl) dibenzo [*b,d*] thiophene 5,5-dioxide (**7**) with a yield of 90%, the related ¹H NMR spectra are shown in Figure S1 (Supporting Information online).

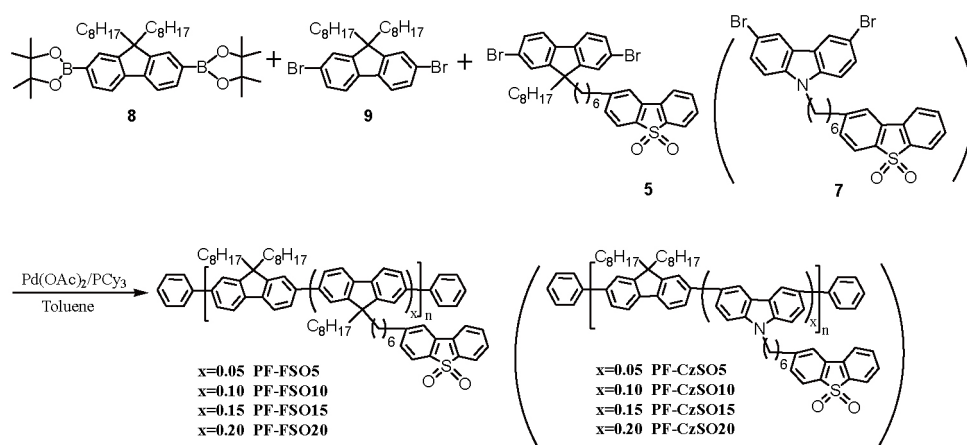
The detailed synthetic routes of polymers are shown in



Scheme 1 Synthetic routes of the monomers.

Scheme 2. Through a palladium catalyzed Suzuki polymerization with molar feed ratios of monomer **8:9:5** of 50:50:0, 50:45:5, 50:40:10, 50:35:15, and 50:30:20, the corresponding polymers were afforded and denoted as **PFO**, **PF-FSO5**, **PF-FSO10**, **PF-FSO15**, and **PF-FSO20**, respectively. Replacing monomer **5** by **7** and with the molar feed ratio of monomer **8:9:7** of 50:45:5, 50:40:10, 50:35:15, 50:30:20, copolymers that denoted as **PF-CzSO5**, **PF-CzSO10**, **PF-CzSO15**, and **PF-CzSO20** were afforded in moderate yields, respectively.

All the resulting copolymers can be easily dissolved in common organic solvents, such as tetrahydrofuran (THF), chloroform (CHCl₃), chlorobenzene and dichlorobenzene at room temperature. The number average molecular weights (M_n) are in the range of 87.9–171.7 kDa with a polydispersity index (PDI) of 1.35–1.90 for **PF-FSOs** and **PF-CzSOs**. The content of SO unit in copolymers were calculated from the results of elemental analysis and listed in **Table 1**. It can be seen that the actual contents of SO unit in polymers are more than the feed ratios, which means that the monomers **5** and **7** own higher reactivity.



Scheme 2 Synthetic routes of the polymers.

Table 1 Molecular weight and thermal properties of the polymers

polymer	M_n ($\times 10^4$)	PDI	SO (mol%) in		T_g ($^{\circ}\text{C}$)	T_{LC} ($^{\circ}\text{C}$)	T_d ($^{\circ}\text{C}$)
			feed ratio	polymer ^{a)}			
PFO	3.05	2.31	0	0	72	140	385
PF-SO10	3.55	1.82	10	8.5	–	156	397
PF-FSO5	10.25	1.64	5	8.9	–	155	411
PF-FSO10	15.62	1.35	10	13.1	79	150	410
PF-FSO15	14.93	1.45	15	16.6	83	148	411
PF-FSO20	11.18	1.68	20	26.5	94	139	412
PF-CzSO5	12.39	1.55	5	7.0	–	–	413
PF-CzSO10	8.79	1.90	10	14.3	–	–	411
PF-CzSO15	16.66	1.47	15	16.1	–	–	405
PF-CzSO20	17.17	1.48	20	25.0	–	–	408

a) Calculated from the elemental analysis data.

3.2 Thermal properties

Thermal properties of the polymers were evaluated by the thermal gravimetric analysis (TGA) measurement. TGA reveals excellent thermal stability of polymers under nitrogen. As shown in **Table 1**, the decomposition temperature (5% weight loss) of the homopolymer **PFO** is 385 $^{\circ}\text{C}$, while those of the copolymers are over 400 $^{\circ}\text{C}$ (Figure S2). Thermally induced phase transition behavior of the polymers was investigated by the differential scanning calorimetry (DSC). **Figure 1** shows the heating curves of polymers **PF-FSOs** (a) and **PF-CzSOs** (b). The glass transition temperatures (T_g) of **PF-FSOs** are in the range of 79–94 $^{\circ}\text{C}$, higher than that of **PFO**. The phase transition peaks from partially crystalline state to liquid crystalline (T_{Cr-LC}) appear around 142 $^{\circ}\text{C}$ for **PFO**, and 139–155 $^{\circ}\text{C}$ for **PF-FSOs** (**Figure 1**(a)). From **Figure 1**(b), it can be seen that no obvious phase transition peak occurred, neither the glass transition nor the partially crystalline state, which indicate the higher degree of irregularity of **PF-CzSOs** backbone, due to the *meta*-linking carbazole unit in the polymer main chain [36].

3.3 Electrochemical properties

Electrochemical properties of the copolymers were examined by cyclic voltammetry (CV). The p-doping and n-doping traces of copolymers are shown in Figure 2, and the detailed electrochemical data are summarized in Table 2. The oxidation potentials of polymers were calibrated by ferrocene/ferrocenium redox couple (Fc/Fc⁺), which was

measured to be 0.49 V. It is assumed that the redox potential of Fc/Fc⁺ has an absolute energy level of 4.8 eV to vacuum [37]. Therefore, the highest occupied molecular orbital (HOMO) and the lowest unoccupied molecular orbital (LUMO) energy levels of the copolymers are calculated according to the equation of $E_{\text{HOMO}} = -e(E_{\text{ox}} + 4.80 - 0.49)$ (eV) and $E_{\text{LUMO}} = -e(E_{\text{red}} + 4.80 - 0.49)$ (eV), where E_{ox} and E_{red} are the onset of the oxidation potentials and reduction potentials

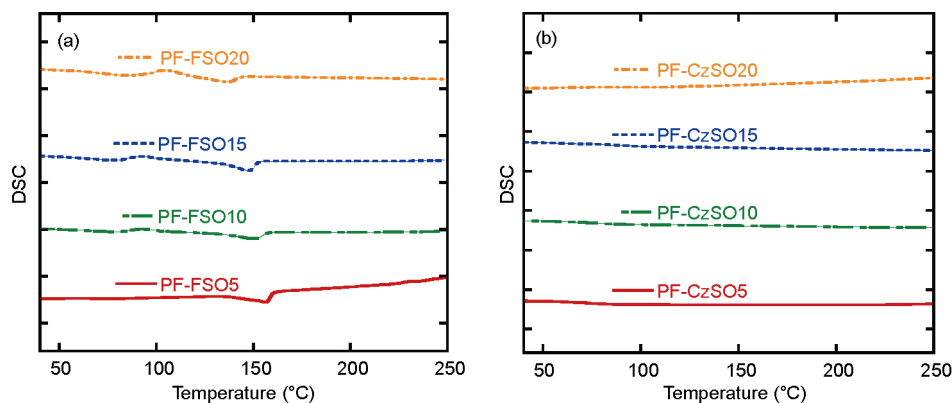


Figure 1 DSC curves of the polymers (color online).

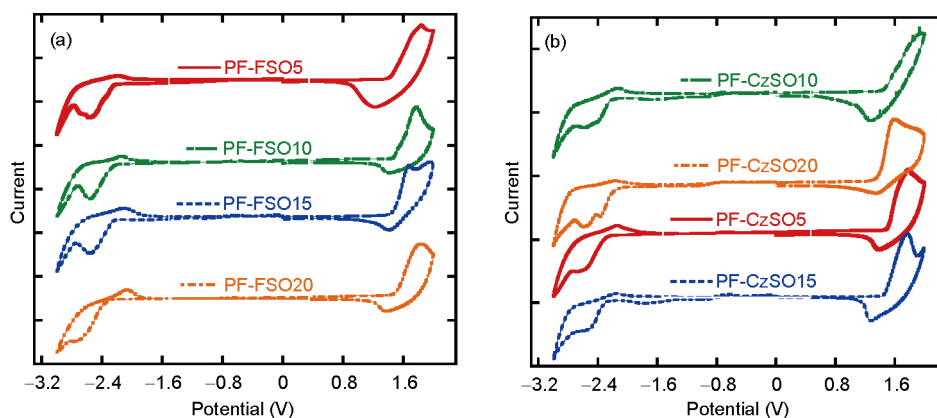


Figure 2 CV curves for PF-FSOs (a) and PF-CzSOs (b) (color online).

Table 2 Photophysical and electrochemical properties of the polymers

sample	E_{ox} (V)	HOMO (eV)	E_{red} (V)	LUMO (eV)	$E_{\text{g}}^{\text{opt a)}$ (eV)	$\lambda_{\text{abs,f}}$ (nm)	$\lambda_{\text{PL,f}}$ (nm)	$Q_{\text{PL}}^{\text{b)}$ (%)
SO	1.6	-6.00	-1.74	-2.57	–	–	–	–
PFO	1.28	-5.68	-2.42	-1.89	3.00	388	425450	32
PF-SO10	1.44	-5.75	-2.19	-2.12	2.90	390	446468	42
PF-FSO5	1.38	-5.69	-2.23	-2.08	2.93	384	426447	48
PF-FSO10	1.46	-5.77	-2.26	-2.05	2.93	385	423447	40
PF-FSO15	1.40	-5.71	-2.28	-2.03	2.93	385	424,449	51
PF-FSO20	1.46	-5.77	-2.36	-1.95	2.93	385	423,445	59
PF-CzSO5	1.44	-5.75	-2.30	-2.08	2.94	382	423,439	34
PF-CzSO10	1.42	-5.73	-2.25	-2.06	2.96	382	423,448	32
PF-CzSO15	1.46	-5.77	-2.34	-1.97	2.96	379	422,447	36
PF-CzSO20	1.37	-5.68	-2.21	-2.10	2.96	375	424,447	66

a) Calculated from the absorption spectra threshold; b) measured in film.

relative to Ag/Ag^+ . The E_{HOMO} and E_{LUMO} of **PF-FSOs** and **PF-CzSOs** are in the range of -5.69 – -5.77 eV and -5.68 – -5.75 eV, -1.95 – -2.08 eV and -1.97 – -2.10 eV, respectively, which slightly decrease with the increase of SO content in side chain.

3.4 Photophysical properties

Figure 3 shows UV-Vis absorption and PL spectra of the polymers in toluene solution. A distinct absorption peak at about 388 nm is attributed to the π - π^* transition of the conjugated fluorene backbone. It should be noted that the absorption spectra of **PF-FSOs** are unchanged with the increasing SO content in side chain, indicating the absorption spectra of polymer are independent on the SO content in side chain (**Figure 3(a)**). While, the **PF-CzSOs** reveal a weak blue-shift absorption due to the *meta*-linking carbazole unit in the polymer backbone (**Figure 3(b)**).

All polymers show well-structured PL spectra with the emission peaked at about 416 nm and a shoulder peaked at about 440 nm in toluene solution, respectively. With the increasing SO content in side chain, the PL emission has no obvious changes, in addition a slight decreased shoulder

peaks for **PF-FSOs**, indicating the SO moiety in alkyl side chain have no contributions to the PL emission of polymers (**Figure 3(a)**). The detailed photophysical results are summarized in **Table 2**. In **Figure S4(a)**, it can be seen that the **PF-FSOs** and **PF-CzSOs** containing SO unit in side chain showed the same spectra with respect to that of **PFO**. Compared with the **PF-SO10** containing SO unit in main chain, the **PF-FSOs** and **PF-CzSOs** containing SO unit in side chain exhibited blue-shifted absorption and narrowing emission spectra (**Figure S4(b)**).

PL spectra of the **PF-FSO20** and **PF-CzSO20** in different polar solution are shown in **Figure 4**, respectively. It can be seen that the PL spectra of copolymers are kept unchanged in toluene, THF and CHCl_3 solution, neither obviously bathochromic shift nor broadening trends. This fact is remarkably different from the polymers containing SO unit in backbone, which show stronger ICT effect [25–28], indicating the unremarkable ICT effect existed in the polymers containing SO unit in alkyl side chain.

Figure 5 shows UV-Vis absorption and PL spectra of the copolymers in film. It can be seen that with the increasing of **FSO** and **CzSO** content, the absorption spectra display unchanged for **PF-FSOs** and a weak blue shift for **PF-CzSOs**,

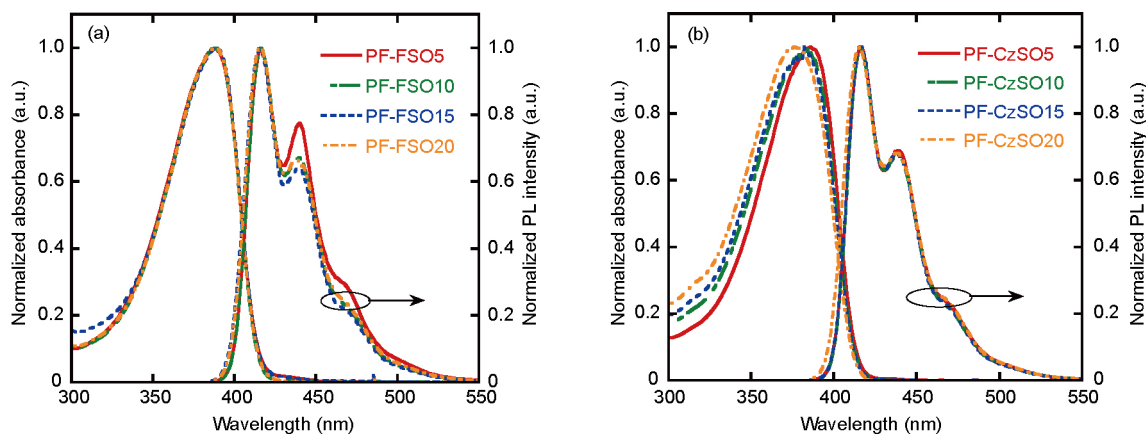


Figure 3 UV-Vis absorption and PL spectra of the polymers **PF-FSOs** (a) and **PF-CzSOs** (b) in toluene solution (color online).

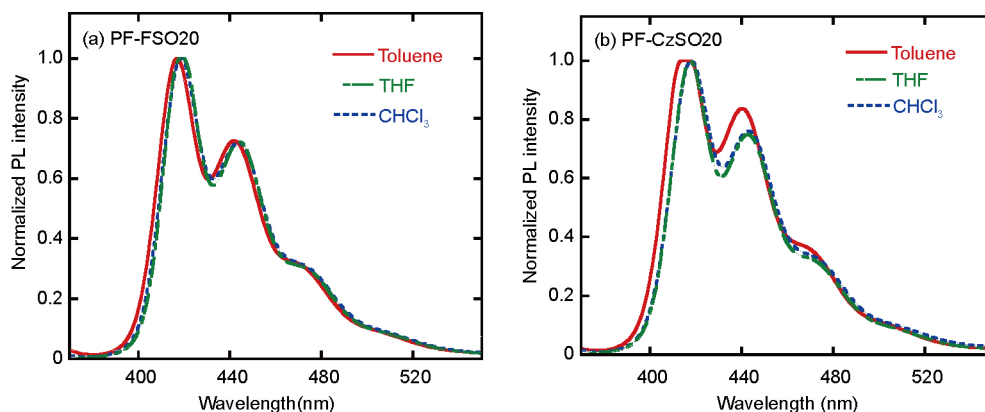


Figure 4 PL spectra of the polymers **PF-FSO20** (a) and **PF-CzSO20** (b) in different polar solution (color online).

respectively. PL spectra of the copolymers show the well-structured local excited (LE) emission, and also no broadenings and redshifts for **PF-FSOs** and **PF-CzSOs**. In Figure S5(a), the **PF-FSO10** and **PF-CzSO10** containing SO unit in side chain show the same spectra with respect to that of **PFO**. Compared with the **PF-SO10** with SO unit in main chain, the **PF-FSO10** and **PF-CzSO10** containing SO unit in side chain exhibit obvious blue-shifted and narrowing emission spectra (Figure S5(b)). The photoluminescence (PL) efficiencies of the polymers are in the range of 40%–59% for **PF-FSOs**, and 32%–66% for **PF-CzSOs**, which are higher than that of **PFO** homopolymer (Table 2).

3.5 Device performances

Electroluminescence of the polymers were evaluated based on the device with a configuration of ITO/PEDOT:PSS/polymer (80 nm)/CsF (1.5 nm)/Al (80 nm). EL spectra of the polymers are shown in Figure 6. It can be seen that the EL spectra of polymers all show a weak hypsochromic shift with the increasing SO unit in side chain. EL spectra of the copolymers compared with **PFO** and **PF-SO10** are shown in Figure 7. It can be seen that EL spectra of the polymers link-

ing SO unit to side chain, **PF-FSO10** and **PF-CzSO10** exhibit a slight blue shift with respect to that of **PFO**, but a remarkable blue shift and narrowing compared with that of the **PF-SO10** containing SO unit in main chain, which could be attributed to both strong steric effect and weak ICT effect on the EL emission existed in the polymers containing SO unit in side chain.

The EL spectra of **PF-FSO15** and **PF-CzSO15** with the variation of current densities are shown in Figure 8. It can be seen that EL spectra of the polymers are almost unchanged in the range of current densities from 100–400 mA cm⁻². It also should be noted that the unexpected low-energy emission band corresponding to the excimers or fluorenone-defects cannot be discerned even at a high current density of 400 mA cm⁻², indicating the superb EL stability of the devices based on the resulted copolymers.

The single layer device performances are summarized in Table 3. It can be seen that the device efficiency of **PFO** exhibits as low as LE_{max} of 0.37 cd A⁻¹. In contrary, the efficiencies of the copolymers have a substantial enhancement with the increasing content of SO unit in side chain, and **PF-FSO15** and **PF-CzSO20** show superior performances, in terms of the LE_{max} of 1.17 and 0.68 cd A⁻¹ with the CIE

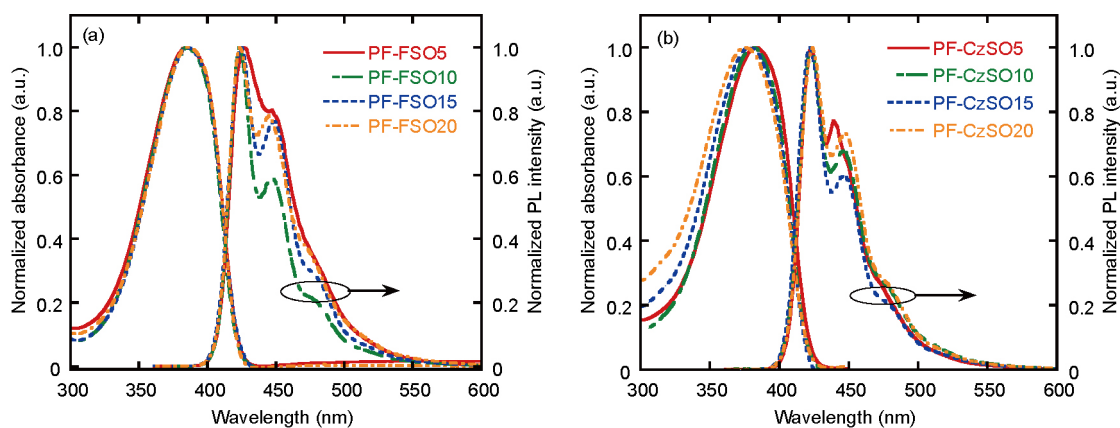


Figure 5 UV-Vis absorption and PL spectra of the polymers **PF-FSOs** (a) and **PF-CzSOs** (b) in film (color online).

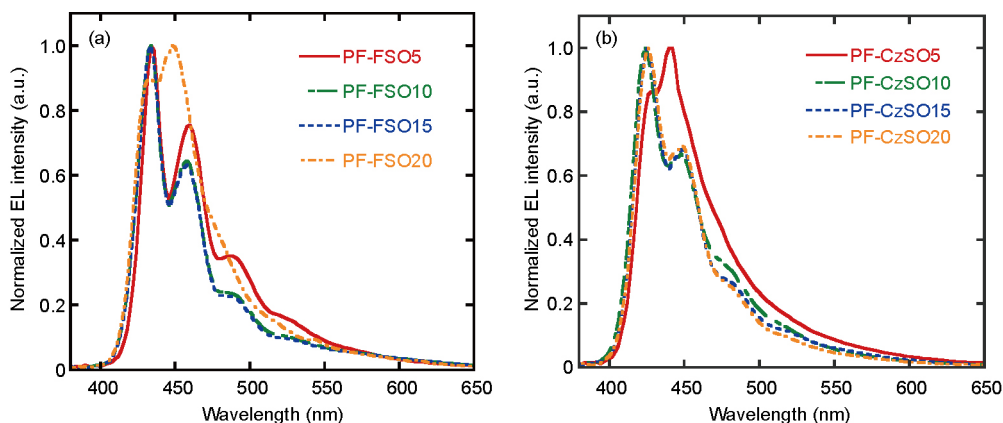


Figure 6 EL spectra of the polymers **PF-FSOs** (a) and **PF-CzSOs** (b) (color online).

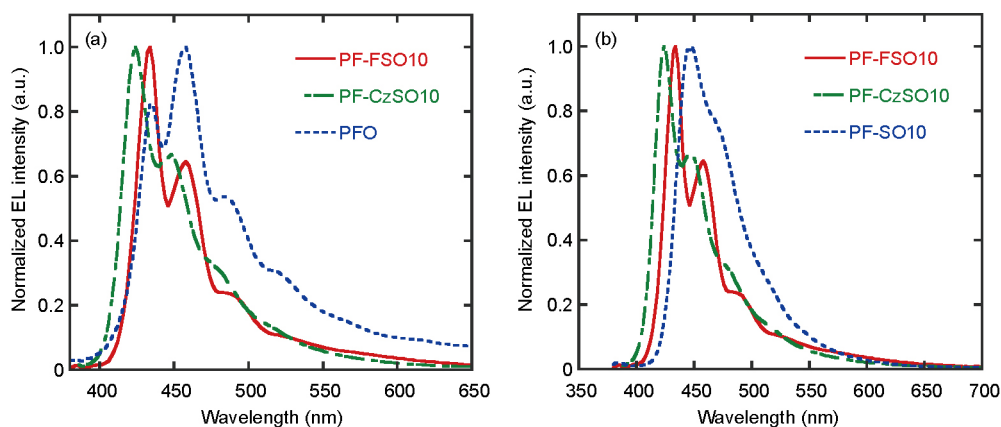


Figure 7 EL spectra of the polymers compared with PFO (a) and PF-SO10 (b) (color online).

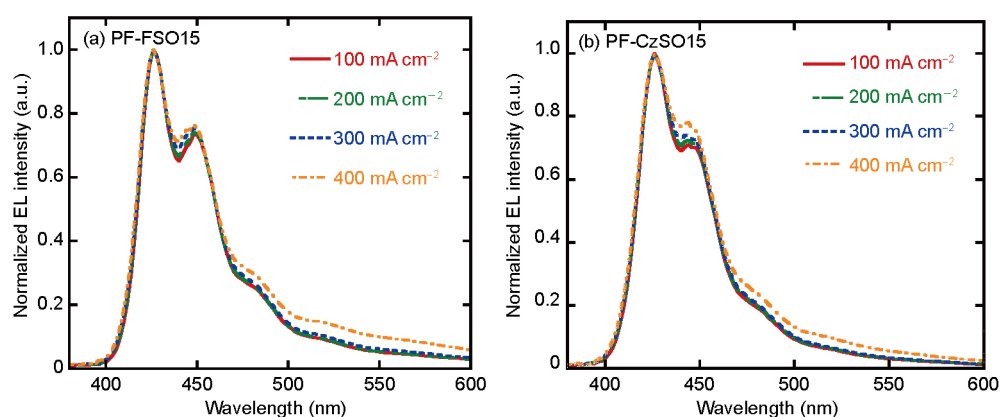


Figure 8 EL spectra of the polymers PF-FSO15 (a) and PF-CzSO15 (b) with the variation of current densities from 100 to 400 mA cm⁻² (color online).

Table 3 Device performances of the polymers^{a)}

polymer	V_{on} (V)	LE_{max} (cd A ⁻¹)	EQE_{max} (%)	L_{max} (cd m ⁻²)	CIE (x,y) ^{b)}
PFO	3.4	0.37	0.42	1934	(0.18, 0.18)
PF-SO10	3.2	2.04	1.46	4296	(0.16, 0.17)
PF-FSO5	3.8	0.74	0.77	3911	(0.17, 0.13)
PF-FSO10	4.6	0.80	0.83	3095	(0.18, 0.11)
PF-FSO15	4.8	1.17	1.10	2002	(0.18, 0.11)
PF-FSO20	4.4	0.70	0.99	1288	(0.17, 0.10)
PF-CzSO5	4.2	0.54	0.56	2837	(0.17, 0.12)
PF-CzSO10	3.8	0.22	0.23	1143	(0.17, 0.11)
PF-CzSO15	3.6	0.51	0.52	1764	(0.17, 0.10)
PF-CzSO20	4.1	0.68	0.71	2075	(0.17, 0.10)

a) The device structure: ITO/PEDOT:PSS/EL/CsF/Al; b) measured at 12 mA cm⁻² current density.

coordinates of (0.18, 0.11) and (0.17, 0.10), respectively. The improved performances could be attributed to the increased PL quantum efficiencies, and might be correlated to more balanced charge carrier transport in the emissive layer (Figure 9(b)).

The single charge carrier devices were fabricated and the current density-electric field characteristics are shown in Figure 9. It is realized that the PFO exhibits the imbalanced

hole/electron fluxes, as the hole mobility is distinctly higher than that of electron mobility in a range of the applied electric fields, which may lead to inferior device performances at the high current densities. In contrast, the well-balanced hole/electron fluxes can be realized for copolymer PF-FSO15, that the hole current decreases 30 times and the electron current increases 15 times at a driving electric field of 2×10^5 (V cm⁻¹). And PF-FSO15 shows the more balanced

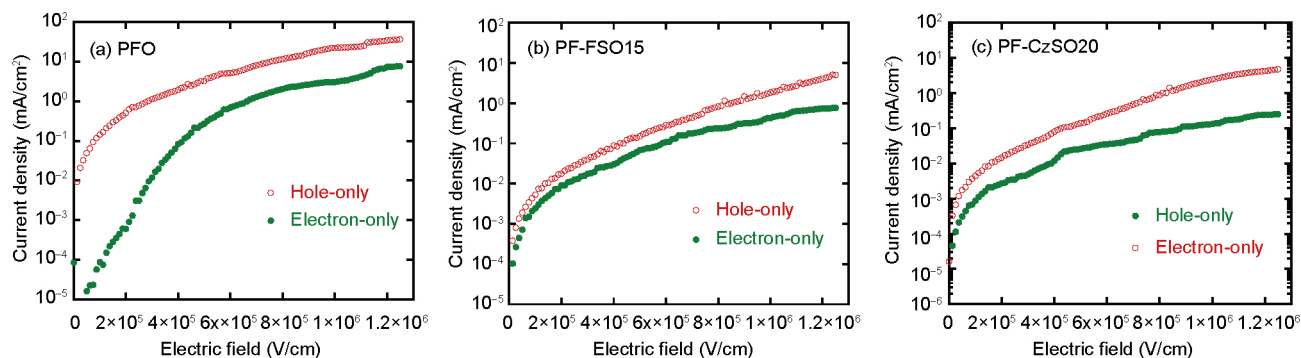


Figure 9 Current densities as a function of electric fields for single carrier devices of PFO (a), PF-FSO15 (b), and PF-CzSO20 (c) (color online).

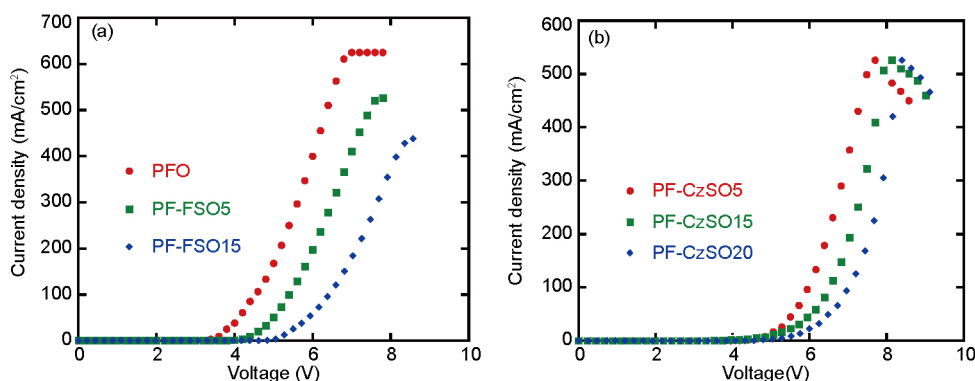


Figure 10 Current density (J)-voltage (V) curves of the PF-FSOs (a) and PF-CzSOs (b) with a configuration of ITO/PEDOT:PSS/EL/CsF/Al (color online).

charge carrier than PF-CzSO20, which could illustrate that PF-FSO20 has a highest PLQY, but with the middle device performances. The fact indicated that linking SO unit to the alkyl side chain of the polyfluorene effectively resulted in the balanced charge carriers across the emissive layer, which can in turn lead to the improved device performances.

In Figure 10, it can be seen that the current densities obviously decrease with the increasing content of SO unit in side chain of the polymers. As we all know, the contact between the hole transporting layer and the emissive layer will be non-ohm contact if the energy gap of HOMO level go beyond 0.3 eV [38]. Considering that the bigger HOMO level gap between PEDOT:PSS (-5.2 eV) and PFO (-5.68 eV), the hole injection should be non-ohm injection. In Table 2, the HOMO level of PF-CzSOs and PF-FSOs are even deeper than that of PFO. Therefore, the PF-CzSOs and PF-FSOs have bigger injection barrier compared with PFO, which will lead to higher turn-on voltages [39]. Furthermore, the packing of polymer chain is disordered and incompact due to the huge steric hindrance introduced by long side chain with SO unit, which decreases the carrier mobility (Figure 9). The decrease of carrier mobility also results in higher turn-on voltage.

The energy levels of materials used in the devices are shown in Figure 11. It can be seen that the SO moiety owns low E_{LUMO} and E_{HOMO} compared with PFO backbone, which

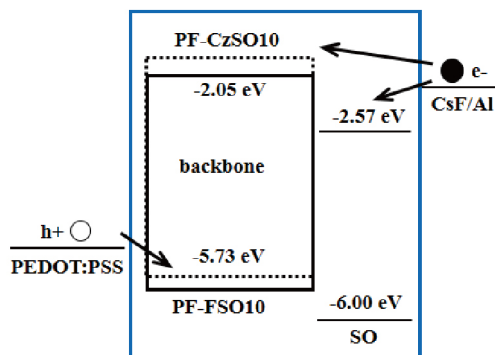


Figure 11 Energy levels of the materials used in the devices (color online).

can be understood as that the attached electron-deficient SO unit can effectively facilitate electron injection from the cathode, and further to PFO backbone, which allow to inject more electrons from the cathode to the polymer main chain and leads to more balanced charge carriers in the device [40].

3.6 Film morphology

AFM measurement was used and the relevant images are shown in Figure 12. We can see that PFO exhibits quite smooth morphology with root-mean-square (RMS) value of 0.53 nm. In contrast, the PF-FSO15 consisting SO unit in

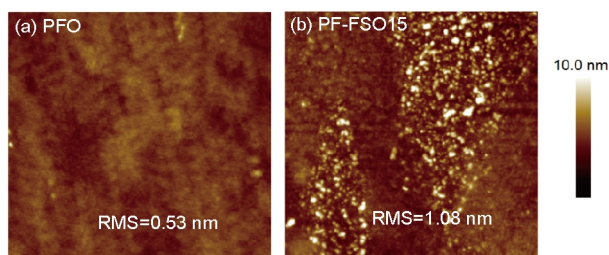


Figure 12 AFM topography ($3\ \mu\text{m}\times 3\ \mu\text{m}$) of PFO (a) and PF-FSO15 (b) (color online).

side chain exhibit rougher morphology, with RMS values of 1.08 nm. The rougher morphology indicates that SO unit in alkyl side chain of the polymers causes disordered packing of the polymer chain, which can potentially facilitate charge injection from the electrodes.

4 Conclusions

In conclusions, the blue light-emitting polyfluorenes (PF-FSOs and PF-CzSOs) containing dibenzothio-phene-*S,S*-dioxide (SO) unit in alkyl side chain were synthesized. The thermal, electrochemical, photophysical and electroluminescent properties of resulting polymers were systematically investigated by comparison with that of PFO and PF-SO10 containing SO unit of 10 mmol% in main chain. The results indicated that introducing SO unit into the alkyl side chain of PFO can restrain the intramolecular charge transfer (ICT) and improve the EL performances. EL spectra of copolymers show high spectra stability with the increase of current densities in the range of 100–400 mA cm⁻².

Acknowledgments This work was supported by the National Key Basic Research and Development Program of China (2015CB655004), the National Natural Science Foundation of China (51473054, 91333206), and the Fundamental Research Funds for the Central Universities, South China of Technology (2017MS020).

Conflict of interest The authors declare that they have no conflict of interest.

- Ying L, Li Y, Wei C, Wang M, Yang W, Wu H, Cao Y. *Chin J Polym Sci*, 2013, 31: 88–97
- Liu SJ, Zhong CM, Zhang J, Duan CH, Wang XH, Huang F. *Sci China Chem*, 2011, 54: 1745–1749
- Zhang XW, Lei ZF, Chen YH, Chen KY, Xu WD, Hao L, Fan QL, Lai WY, Huang W. *RSC Adv*, 2016, 6: 10326–10333
- Lai WY, Liu D, Huang W. *Sci China Chem*, 2010, 53: 2472–2480
- Guan R, Xu Y, Ying L, Yang W, Wu H, Chen Q, Cao Y. *J Mater Chem*, 2009, 19: 531–537
- Guo T, Yu L, Yang Y, Li Y, Tao Y, Hou Q, Ying L, Yang W, Wu H, Cao Y. *J Lumin*, 2015, 167: 179–185
- Qiao Z, Cao DR, Liu QL, Weng JN, He ZC, Han SH, Peng JB. *Sci China Ser B-Chem*, 2009, 52: 2038–2042
- Zhu M, Yang C. *Chem Soc Rev*, 2013, 42: 4963–4976
- Jin G, Xia L, Liu Z, Lin H, Ling J, Wu H, Hou L, Mo Y. *J Mater Chem C*, 2016, 4: 905–913
- Wang M, Li Y, Xie ZY, Wang LX. *Sci China Chem*, 2011, 54: 656–665
- Liu C, Li Y, Li Y, Yang C, Wu H, Qin J, Cao Y. *Chem Mater*, 2013, 25: 3320–3327
- Cook JH, Santos J, Al-Attar HA, Bryce MR, Monkman AP. *J Mater Chem C*, 2015, 3: 9664–9669
- Knaapila M, Monkman AP. *Adv Mater*, 2013, 25: 1090–1108
- Gong X, Iyer PK, Moses D, Bazan GC, Heeger AJ, Xiao SS. *Adv Funct Mater*, 2003, 13: 325–330
- Lu HH, Liu CY, Chang CH, Chen SA. *Adv Mater*, 2007, 19: 2574–2579
- King SM, Perepichka II, Perepichka IF, Dias FB, Bryce MR, Monkman AP. *Adv Funct Mater*, 2009, 19: 586–591
- Schelkle KM, Bender M, Jeltsch K, Buckup T, Müllen K, Hamburger M, Bunz UHF. *Angew Chem Int Ed*, 2015, 54: 14545–14548
- Gopikrishna P, Das D, Iyer PK. *J Mater Chem C*, 2015, 3: 9318–9326
- Lee JF, Hsu SLC. *Polymer*, 2009, 50: 5668–5674
- Li JY, Ziegler A, Wegner G. *Chem Eur J*, 2005, 11: 4450–4457
- Perepichka II, Perepichka IF, Bryce MR, Pålsson LO. *Chem Commun*, 2005, 11: 3397
- Huang TH, Whang WT, Shen JY, Wen YS, Lin JT, Ke TH, Chen LY, Wu CC. *Adv Funct Mater*, 2006, 16: 1449–1456
- Ye J, Zheng CJ, Ou XM, Zhang XH, Fung MK, Lee CS. *Adv Mater*, 2012, 24: 3410–3414
- Romain M, Quinton C, Tondelier D, Geffroy B, Jeannin O, Rault-Berthelot J, Poriel C. *J Mater Chem C*, 2016, 4: 1692–1703
- Hsu CY, Hsieh MT, Tsai MK, Li YJ, Huang CJ, Su YK, Whang TJ. *Tetrahedron*, 2012, 68: 5481–5491
- Hsiao SH, Wu LC. *Dyes Pigments*, 2016, 134: 51–63
- Li Y, Wu H, Zou J, Ying L, Yang W, Cao Y. *Org Electron*, 2009, 10: 901–909
- Liu J, Hu S, Zhao W, Zou Q, Luo W, Yang W, Peng J, Cao Y. *Macromol Rapid Commun*, 2010, 31: 496–501
- He R, Hu S, Liu J, Yu L, Zhang B, Li N, Yang W, Wu H, Peng J. *J Mater Chem*, 2012, 22: 3440–3446
- Yu L, Liu J, Hu S, He R, Yang W, Wu H, Peng J, Xia R, Bradley DDC. *Adv Funct Mater*, 2013, 23: 4366–4376
- Guo T, Yu L, Zhao B, Ying L, Wu H, Yang W, Cao Y. *J Polym Sci Part A-Polym Chem*, 2015, 53: 1043–1051
- Hu L, Yang Y, Xu J, Liang J, Guo T, Zhang B, Yang W, Cao Y. *J Mater Chem C*, 2016, 4: 1305–1312
- Zhao S, Liang J, Guo T, Wang Y, Chen X, Fu D, Xiong J, Ying L, Yang W, Peng J, Cao Y. *Org Electron*, 2016, 38: 130–138
- Guo T, Zhong W, Zhang A, Zou J, Ying L, Yang W, Peng J. *New J Chem*, 2016, 40: 179–186
- Xu J, Yang Y, Hu L, Guo T, Zhang B, Yang W, Cao Y. *Dyes Pigments*, 2017, 138: 245–254
- Scherf U, List EJW. *Adv Mater*, 2002, 14: 477–487
- Oguzhan E, Bilgili H, Baycan Koyuncu F, Ozdemir E, Koyuncu S. *Polymer*, 2013, 54: 6283–6292
- Liaptsis G, Meerholz K. *Adv Funct Mater*, 2013, 23: 359–365
- Park J, Lee C, Jung J, Kang H, Kim KH, Ma B, Kim BJ. *Adv Funct Mater*, 2014, 24: 7588–7596
- Huang CW, Tsai CL, Liu CY, Jen TH, Yang NJ, Chen SA. *Macromolecules*, 2012, 45: 1281–1287